Dynamic and Control Simulation of Rotor Suspended by Three Radial AMBs Based on Multibody Dynamics

Yixin Su [a], Yichen Yao [a,c], Yanhui Ma [a], Hongwei Li [b], Wentao Yu [b], Suyuan Yu [a*]

[a] Department of Energy and Power Engineering, Tsinghua University, Beijing, China, suyuan@tsinghua.edu.cn
[b] School of Electrical Engineering, Shandong University, Jinan, China
[c] School of Energy and Environment, Southeast University, Nanjing, China

***Abstract*— Multiple AMBs have greater bearing capacities than two radial AMBs but the multiple AMBs affect the system dynamics and control characteristics. The dynamic equations were developed for a three radial AMB system to calculate the critical speed and the unbalanced response of the three radial AMB system which are compared with those of a two AMB system. The model accounts for bearing misalignment and the effect of different support locations. The model is a flexible rotor with discs including a rigid body and Euler-Bernoulli beam based on an absolute nodal coordinate formulation and constraints based on the first type of Lagrange equation. The electromagnetic force on the AMB at each DOF is controlled by a PID control law in real time. The governing equations including the constraint equations are solved by the available differential algebraic equation solver.**

I. INTRODUCTION

Rotors are normally supported by two radial active magnetic bearings (AMBs) in maglev rotating machinery. However, multiple radial AMBs are required when the rotor is slender such as in aero-engines, large steam turbines, ship shafts and helicopter shafts. Multiple AMB systems have greater bearing capacity than two AMB systems but the dynamics and control characteristics of the system are much more complicated.

Multiple radial AMB systems are statically indeterminate systems. DeSmidt et al. [1] used three AMBs to support helicopter tail rotors. The system stability was controlled by the AMB that suppressed the vibrations caused by the rotor imbalance. However, the design neglected the bearing misalignment because of the use of a universal joint. Zhao et al. [2] and Cai [3] added a third radial AMB to an AMB-rotor system, but this bearing only provided damping without stiffness. Liu et al. [4-5] added various numbers of AMBs to a bearing-rotor system. They first studied the influence of the bearing misalignment when the sensor zero position was not changed with the magnetic bearing modeled as an equivalent spring. Then, a PID controller was used to control the linearized electromagnetic force with the responses for step and sinusoidal excitation compared when the sensor zero position was not changed. They did not investigate the influence of the addition of multiple radial AMBs on the system controllability and observability or the effect of different support locations.

Unlike with rotors supported by multiple mechanical bearings, multiple radial AMB systems can eliminate bearing loads caused by bearing misalignment by adjusting the zero position of the displacement sensor. However, the equivalent bearing stiffness changes with changes in the static balance position. However, active controllability makes the rotor dynamics analysis much more difficult because the dynamic characteristics of the system are closely related to the control law. With flexible rotor, even when the controller is known and has the simple structure such as a PID controller, the closed-loop AMB support parameters cannot be easily extracted from the closed-loop transfer function. [6]

This article considers a three radial AMB system applied to a flexible rotor model with discs including a rigid body, Euler Bernoulli beam and constraints. The model is based on the first type of Lagrange equation. The beam element that is based on an absolute nodal coordinate formulation (ANCF) allows arbitrary spatial rigid motion, large bending, extension and torsion deformation [7]. The electromagnetic force on the AMB at each DOF is controlled by the PID control law in every calculational step. The effect of the bearing misalignment is simulated by changing the static balance positions of the objects. The model is used to predict the critical speed and unbalanced response for various support locations.

II. MATHEMATICAL MODEL

A. Dynmics equations of the ANCF beam

The Euler Bernoulli beam elements based on the absolute nodal coordinate formulation (ANCF) proposed by Zhao et al. [7] are used to model the flexible rotor. This model allows arbitrary spatial rigid motion, large bending, extension and torsion deformation. As shown in Fig. 1, the Euler-Bernoulli beam has a rigid cross section which remains perpendicular to the tangent of the centerline during deformation. The generalized elemental coordinates, $\mathbf{q}_e$, and the generalized coordinates of nodes Ⅰ and Ⅱ are:

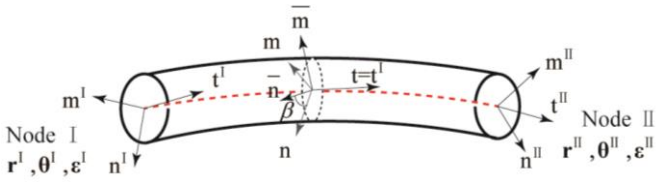

Figure 1. Euler Bernoulli beam elements based on the absolute nodal coordinate formulation (ANCF)

$$\mathbf{q}_e=\begin{bmatrix}\mathbf{q}^{\mathrm{I}}\\ \mathbf{q}^{\mathrm{II}}\end{bmatrix}\quad \mathbf{q}^{\mathrm{I}}=\begin{bmatrix}\mathbf{r}^{\mathrm{I}}\\ \boldsymbol{\theta}^{\mathrm{I}}\\ \boldsymbol{\varepsilon}^{\mathrm{I}}\end{bmatrix}\quad \mathbf{q}^{\mathrm{II}}=\begin{bmatrix}\mathbf{r}^{\mathrm{II}}\\ \boldsymbol{\theta}^{\mathrm{II}}\\ \boldsymbol{\varepsilon}^{\mathrm{II}}\end{bmatrix} \tag{1}$$

Where, $\mathbf{r}$ is the global displacement vector of the node, $\boldsymbol{\varepsilon}$ is the normal strain at the neutral axes and $\begin{bmatrix}\mathbf{l} & \mathbf{m} & \mathbf{n}\end{bmatrix}$ is the material reference frame. $\boldsymbol{\theta}$ are the Euler parameters or quaternion which satisfy:

$$\mathbf{C}(\mathbf{q}_e)=\begin{bmatrix}\boldsymbol{\theta}^{\mathrm{I}}\boldsymbol{\theta}^{\mathrm{I}} & -1\\ \boldsymbol{\theta}^{\mathrm{II}}\boldsymbol{\theta}^{\mathrm{II}} & -1\end{bmatrix}=\mathbf{0} \tag{2}$$

The mass matrix is given by:

$$\mathbf{M}=\rho L\int_0^l\left[A\left(\frac{\partial\mathbf{r}}{\partial\mathbf{q}_e}\right)^T\left(\frac{\partial\mathbf{r}}{\partial\mathbf{q}_e}\right)+4\left(\frac{\partial\boldsymbol{\theta}}{\partial\mathbf{q}_e}\right)^T\bar{\mathbf{E}}^T\mathbf{J}\bar{\mathbf{E}}\left(\frac{\partial\boldsymbol{\theta}}{\partial\mathbf{q}_e}\right)\right]d\xi \tag{3}$$

Where,

$$\bar{\mathbf{E}}=\begin{bmatrix}-\theta_1 & \theta_0 & \theta_3 & -\theta_2\\ -\theta_2 & -\theta_3 & \theta_0 & \theta_1\\ -\theta_3 & \theta_2 & -\theta_1 & \theta_0\end{bmatrix}$$

$$\mathbf{J}=diag\begin{bmatrix}J_T & J_{yy} & J_{zz}\end{bmatrix}$$

J_T is the rotational inertia and J_{yy} and J_{zz} are the two inertias with respect to the two principal axis $\mathbf{m}$ and $\mathbf{n}$. L is the initial length, ρ is the material density and ξ is the isoparametric coordinate.

The elastic potential work is

$$U=\frac{1}{2}L\int_0^l\left(EA\varepsilon^2+GJ_Tk_1^2+GJ_{22}k_2^2+GJ_Tk_3^2\right)d\xi \tag{4}$$

Where, E and G are the elastic and shear moduli. k_1,k_2,k_3 are the torsion and the two bending curvatures.

The resulting governing equations for the ANCF beam are

$$\begin{cases}\mathbf{M}\ddot{\mathbf{q}}_e+\mathbf{V}\dot{\mathbf{q}}_e+\dfrac{\partial U}{\partial\mathbf{q}_e}+\left(\dfrac{\partial\mathbf{C}}{\partial\mathbf{q}_e}\right)^T\boldsymbol{\lambda}=0\\ \mathbf{C}(\mathbf{q}_e)=0\end{cases} \tag{5}$$

Where,

$$\mathbf{V}=\frac{\partial(\mathbf{M}\dot{\mathbf{q}}_e)}{\partial\mathbf{q}_e}-\frac{1}{2}\left(\frac{\partial(\mathbf{M}\dot{\mathbf{q}}_e)}{\partial\mathbf{q}_e}\right)^T$$

$\boldsymbol{\lambda}$ is the Lagrange multiplier vector.

B. *Dynamics equations of the rigid bodies*

The position coordinate $\mathbf{r}_d$ of a rigid body mass center in the global coordinate system is defined as the generalized coordinate of the rigid body and the unit quaternion $\boldsymbol{\theta}_d$ is defined based on Euler's rotation theorem.

Using the derivation of the first type of Lagrange equation, the dynamics equation of the rigid body can be expressed as [8]:

$$\begin{cases}\mathbf{M}_d\ddot{\mathbf{r}}_d-\mathbf{F}_d=0\\ 4\mathbf{G}_d^T\mathbf{J}_d\mathbf{G}_d\ddot{\boldsymbol{\theta}}_d-8\dot{\mathbf{G}}_d^T\mathbf{J}_d\mathbf{G}_d\dot{\boldsymbol{\theta}}_d+2\boldsymbol{\theta}_d\boldsymbol{\lambda}_d-\mathbf{Q}_d=0\\ \boldsymbol{\theta}_d^T\boldsymbol{\theta}_d-1=0\end{cases} \tag{6}$$

Where $\mathbf{M}_d$ and $\mathbf{J}_d$ are the mass matrix and the inertia matrix of the body, $\mathbf{F}_d$ and $\mathbf{Q}_d$ are the generalized external force and moment, $\boldsymbol{\lambda}_d$ is the Lagrange multiplier, and $\mathbf{G}_d$ is a matrix of the quaternion with the same form as $\bar{\mathbf{E}}$.

C. *Steam turbine rotor model*

A steam turbine rotor supported by three radial AMBs and one axial AMB can be modeled using ANCF beam elements with different sections and rigid parts as shown in Fig. 2. The electromagnetic forces of the AMB at each DOF are applied to the red nodes. The axial motion of the rotor is also taken into consideration.

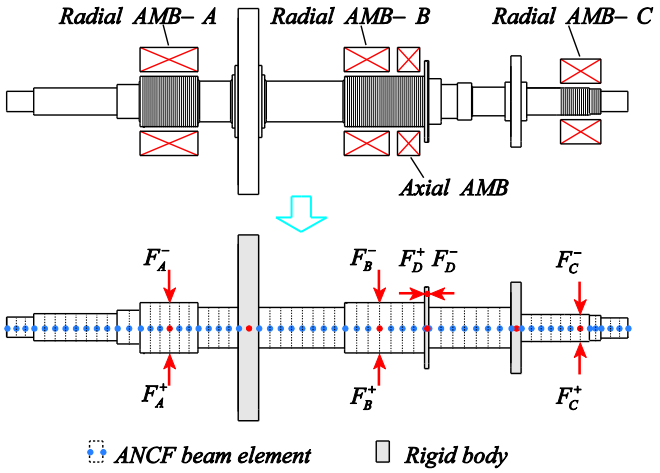

Figure 2. Steam turbine rotor model using ANCF beams and rigid bodies.

The dynamics equation of the rotor system is then obtained based on Eq. 5 and Eq. 6. The governing equations are differential algebraic equations (DAEs) which were solved using the implicit first-order backward differentiation formula (BDF) method. [9]

D. *Controller transfer function*

PID control is most commonly used in industry. In this model, the electromagnetic force of the AMB at each DOF was controlled by a PID control law at each calculational step during the solution. The bearing misalignment was e. The

transfer function for the electromagnetic force and the rotor displacement at each DOF is:

$$T(s) = k_X - G_S(s)G_C(s)G_A(s)k_I \tag{7}$$

Where,

$$G_C(s) = k_p + \frac{k_i}{s} + \frac{k_d s}{1+sT_d}$$

$$G_S(s) = \frac{A_s}{1+T_s s}$$

$$G_A(s) = \frac{\alpha_a}{1+sT_a}$$

k_X is the force displacement coefficient, k_I is the current displacement coefficient. A_s are displacement sensor gain coefficient and A_s, α_a is the power amplifier gain coefficient. T_s and T_a are the attenuation time constants of the displacement sensor and the power amplifier. k_p, k_i, k_d are the PID parameters.

k_X and k_I vary with the static balance position and are related to the bearing misalignment as:

$$k_X = \frac{k}{1-\bar{e}^2}\frac{i_0^2}{s_0^3} \tag{8}$$

$$k_I = \frac{k}{1-\bar{e}^2}\frac{i_0}{s_0^2} \tag{9}$$

Where,

$$\bar{e} = \frac{e}{s_0}$$

$$k = \mu_0 N^2 A$$

s_0 is the uniform gap in the AMB when the rotor is in the ideal center. i_0 is the bias current. μ is the vacuum permeability. N is the number of coil turns. A is the magnetic pole area.

III. Simulations and Discussion

The mathematical model was used to predict the critical speed and the unbalanced response of the rotor supported in three different ways:

(a) Two isotropic radial AMBs at A and C.

(b) Three isotropic radial AMBs at A, B and C

(c) Two isotropic radial AMBs at A and C with one misaligned AMB at B.

Table 1. Simulation conditions

Term	Value	Meaning
$\Delta(kg \cdot m)$	0.001	Unbalanced amount
$\varphi(rad)$	$\pi/3$	Initial phase
$s_0(m)$	1.5×10^{-4}	Gap between AMB and rotor
$e(m)$	1×10^{-4}	Misalignment

Other assumed conditions are listed in Table 1. The steam turbine rotor was modeled using 62 ANCF beam elements and three rigid parts. The three support points are shown in Fig. 2. Nodes 21, 39 and 57 were electromagnetic force support points. Node 30, which had the largest disc, was the unbalanced quantity.

The AMB control parameters were the same at each DOF. The unbalanced responses of the flexible rotor for the three conditions are plotted in Fig. 3 for speeds of 0-4000 rad/s with the PID controller. The figures show the steady-state response of a node on the rotor in the radial direction at different rotational speeds. The physical meaning of the amplitude is the distance between the rotor's axis and its initial position at steady state.

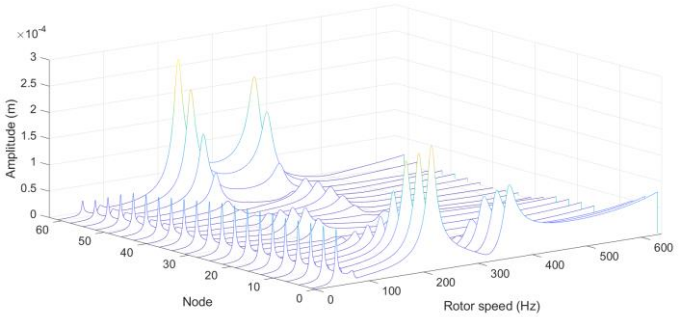

(a) Unbalanced response of the rotor for condition (a)

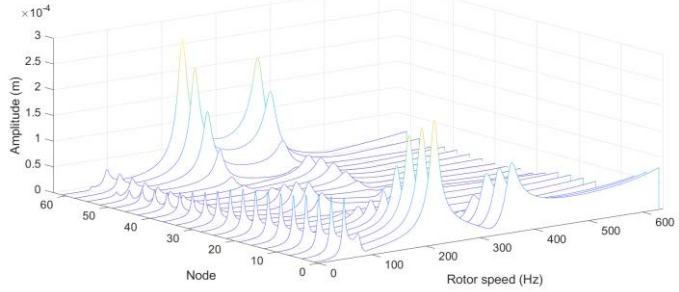

(b) Unbalanced response of the rotor for condition (b)

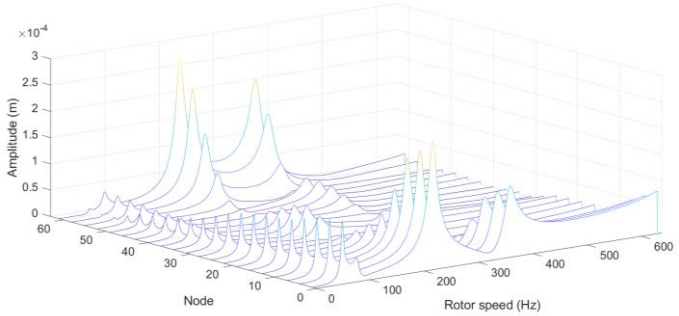

(c) Unbalanced response of the rotor for condition (c)

Figure 3. Unbalanced responses of the rotor for the three support conditions

The vibrational mode of the rotor can be seen in Fig. 3. The flexible mode is almost the same for the three support

conditions. However, the additional AMB at position B changes the rigid mode. The bearing misalignment at position B has little effect on the critical speed.

The rotational speeds corresponding to the peak amplitudes are the critical speeds. Each support condition has the four critical speeds listed in Table 2. The first two are for the rigid modes while the next two are for the flexible modes.

Table 2. Critical speeds (Hz)

Type	Rigid		Flexible	
	1	**2**	**1**	**2**
(a)	46.31	76.08	221.9	361.6
(b)	55.23	83.72	222.7	361.9
(c)	56.02	84.51	222.8	361.9

Table 2 shows that the flexible critical speeds do not change for the three support conditions. In addition, the rigid critical speeds of the three radial AMBs systems are higher than for the traditional two radial AMB system. The results also show that the bearing misalignment at position B has little effect on the critical speed.

The effect of adding an AMB at various support locations was investigated by calculating the dynamic response with an AMB at various locations. The critical speeds vary with the support position as shown in Fig. 4.

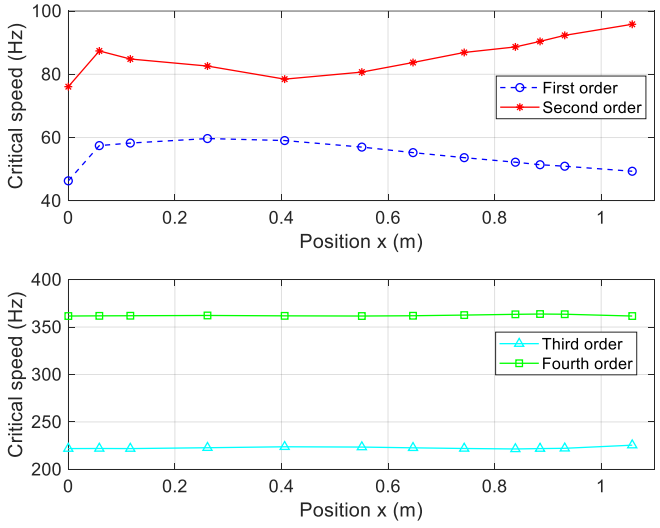

Figure 4. Critical speeds for various suport position

In Fig. 4, x is the distance between the added support point and point A. Thus, $x = 0$ is the traditional two radial AMB system. The upper part of Fig. 4 shows the rigid critical speeds while the lower figure shows the flexible critical speeds. The additional AMB mainly changes the rigid critical speeds. The maximum critical speed of the first order mode is increased by a maximum of 28.87% while the maximum critical speed of the second order mode is increased by a maximum of 25.87%.

The unbalanced response was also evaluated by numerically calculating the transient response in the time domain of each node on the rotor with two or three radial AMBs. The critical speeds of node 21, the node at AMB support point A, were found to be 46.31 Hz and 55.23 Hz as plotted in Fig. 5.

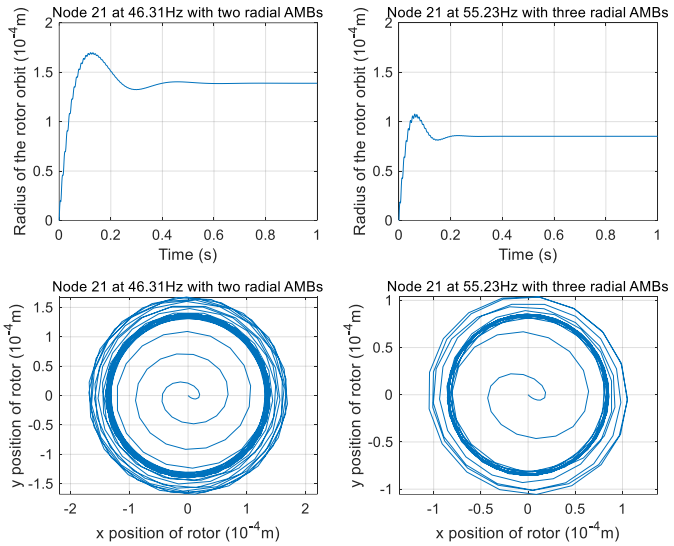

Figure 5. Rotor orbit of Node 21 at 55.23 Hz with two and three radial AMBs

The diagrams in the first row of Fig. 5 show that the forward whirl radius of the rotor orbit changes with time. Node 21 with two radial AMBs tends to steady state after about 0.4 seconds. However, node 21 with three radial AMBs tends to steady state after only about 0.2 seconds. The stable radius of the rotor orbit with three radial AMBs system is $0.8519\times10^{-4}m$ which is less than the radius of $1.389\times10^{-4}m$ with two radial AMBs.

The diagrams in the second row show the rotor orbit with the node initially at the origin. At steady-state, the rotor orbit tends to a circle because of the isotropic system.

These results are consistent with the steady state result plotted in Fig. 3, which validates the results of the unbalanced response calculation.

The controllability and observability of two, three and four radial AMB systems were calculated by Li [10] using the Gram matrix. The results show that the controllability and observability of the four radial AMB system are superior to those of the three radial AMB system with those being superior to those of the two radial AMB system for each mode.

IV. CONCLUSIONS

Models of rotor-bearing systems with two or three radial AMBs were developed based on the first type of Lagrange equation and a real-time PID controller model using ANCF beam elements. The model took into account the time lags of the sensors and the power amplifier and the bearing misalignment.

The model was used to predict the critical speed and the unbalanced response of a rotor supported in three different ways. The results show that adding an AMB to a traditional two radial AMB system will change the rigid mode and the rigid critical speed. The critical speeds differ for different support positions. The maximum critical speed of the first order mode is increased by a maximum of 28.87% while the maximum critical speed of the second order mode is increased by a maximum of 25.87%. Finally, a transient response analysis of a node in the time domain validates the results of the unbalanced response calculations.

V. ACKNOWLEDGMENTS

The authors thank the Laboratory of Multibody Dynamics, Tsinghua University for their support and cooperation. The authors thank Prof. Gexue Ren, Zhihua Zhao and Dr. Jiawei He for providing the multibody dynamics simulation software INSIDES which was used to model the steam turbine rotor.

REFERENCES

[1] Hans A. DeSmidt, K. W. Wang and Edward C. Smith, "Multiharmonic adaptive vibration control of misaligned driveline via Active Magnetic Bearings," *Journal of Dynamic Systems, Measurement, and Control*, vol. 30, no. 4, pp. 41-60, 2008.

[2] Zhao Qianquan and Xie Zhenyu, "Analysis of Dynamic Characteristics of Three Bearing Magnetic Bearing Rotor System," *Machinery Manufacturing and Automation*, vol. 37, no. 2, pp. 31-33, 2008. (in Chinese)

[3] Cai Yongfei, "Research on vibration control of magnetic suspension flexible rotor by passive magnetic suspension damper," Master Thesis, Beihang University, Beijing, China, 2010.

[4] Liu Cong and Xu Longxiang, "Dynamic characteristics of rotor system with multiple magnetic bearings," *Mechanical design and manufacture*, vol. 3, pp. 19-23, 2015. (in Chinese)

[5] Liu Cong, "Research on rotor system supported by multiple magnetic bearings," Master Thesis, Nanjing University of Aeronautics, Nanjing, China, 2015.

[6] Zhou, J., Di, L., Cheng, C. et al, "A rotor unbalance response based approach to the identification of the closed-loop stiffness and damping coefficients of active magnetic bearings," *Mechanical Systems and Signal Processing*, vol. 66, no. 67, pp. 665–678, 2015.

[7] Zhao Z. and Ren G., "A quaternion-based formulation of Euler-Bernoulli beam without singularity," *Nonlinear Dynamics*, vol. 67, no.3, pp. 1825–1835, 2012.

[8] Ma, Y., Hong, D., Cheng, Z. et al, "A multibody dynamic model of the drilling system with drilling fluid," *Advances in Mechanical Engineering*, vol. 8, no. 7, pp. 1–16, 2016.

[9] Wang NY, Cheng ZB, Lu YJ, et al. "A multibody dynamic model of contact between the drillstring and the wellbore and the rock penetration process," *Advances in Mechanical Engineering*, vol. 7, no. 5, pp. 1–12, 2015.

[10] Li Hongwei, "Performance of the Active Magnetic Bearing - Flexible Rotor System for HTR-10GT, " PhD Thesis. Tsinghua University, Beijing, China. 2008.